energy&fuels

Article

pubs.acs.org/EF

Effect of Unsaturated Bond on NO_x and PAH Formation in *n*-Heptane and 1-Heptene Triple Flames

X. Han, S. K. Aggarwal,* and K. Brezinsky

Department of Mechanical and Industrial Engineering, University of Illinois at Chicago, Chicago, Illinois 60607, United States

ABSTRACT: Various engine and shock tube studies have observed increased NO_x emissions from the combustion of biodiesels relative to regular diesel and linked them to the degree of unsaturation or the number of double bonds in the molecular structure of long-chain biodiesel fuels. We report herein a numerical investigation on the structure and emission characteristics of triple flames burning *n*-heptane and 1-heptene fuels, which represent, respectively, the hydrocarbon side chain of the saturated (methyl octanoate) and unsaturated (methyl octenoate) biodiesel surrogates. Our objective is to examine the effect of unsaturated (double) bond on NO_x and soot emissions in a flame environment containing regions of lean premixed, rich premixed, and nonpremixed combustion. A validated detailed kinetic model with 198 species and 4932 reactions was used to simulate triple flames in a counterflow configuration with different levels of premixing and strain rates. Results indicate that although the global structures of *n*-heptane and 1-heptene triple flames are quite similar, there are significant differences with respect to NO_x and polycyclic aromatic hydrocarbon (PAH) emissions from these flames. The NO_x production rates in the rich premixed, lean premixed, and nonpremixed zones are higher in 1-heptene flames than in *n*-heptane flames, and the differences become more pronounced as the level of premixing is increased. The NO_x formed through the prompt, thermal, N_2O, and NNH mechanisms is also higher in 1-heptene flames. NO_x formation in the rich premixed zone is primarily due to the prompt NO, that in the nonpremixed zone is through the thermal NO, and that in the lean premixed zone is due to the NNH and N_2O routes. The PAH species are mainly formed in the rich premixed zone, and their emissions are significantly higher in 1-heptene flames than in *n*-heptane flames. The reaction pathway analysis indicated that the dominant path for benzene formation involves the recombination of two propargyl (C_3H_3) radicals, and the presence of the double bond in 1-heptene provides a significant route for its production through the formation of C_3H_5. This path is not favored in the oxidation of *n*-heptane, as it decomposes directly to smaller alkyl radicals. Whereas the NO_x and PAH emissions decrease with the increase in strain rate, they are consistently higher in 1-heptne flames than in *n*-heptane flames, irrespective of the strain rate.

1. INTRODUCTION

Biodiesel fuels have attracted significant interest due to their potential as a renewable fuel. Moreover, numerous flame and engine studies[1,2] have reported noticeable reductions in the emissions of CO, unburned hydrocarbons, and particulate matter (PM) from the combustion of biodiesel fuels compared to those from conventional diesel, although NO_x emission has generally been found to increase. Some recent investigations have focused on identifying the chemical and physical processes associated with this increased NO_x. An important characteristic of biodiesels, produced from the transesterification of vegetable oils and animal fat, is the existence of double and triple bonds in their molecular structure. The chain length and unsaturated bonds in the fuel molecular structure are known to have a significant influence on the fuel combustion chemistry and, thereby, on the combustion characteristics, including ignition delay, flame speed, and pollutant emissions.

McCormick et al.[3] performed engine tests using several biodiesel fuels from different feedstocks and observed higher NO_x emissions as the fatty acid chain length and the number of double bonds were increased, although there was no significant change in PM emissions. In contrast, Lapuerta et al.[4] observed noticeable reductions in PM emissions with the number of double bonds or degree of unsaturation in the fuel molecular structure, whereas Puhan et al.[5] reported increased emissions of NO_x, smoke, CO, and unburned hydrocarbons (UHCs) with the degree of unsaturation, on the basis of their single-cylinder engine experiments with linseed, jatropha, and coconut oils. Schönborn et al.[6] reported similar results for fatty acid alkyl esters, that is, higher PM emissions with the increase in the number of double bonds. Benjumea et al.[7] conducted single-cylinder engine experiments with three different mixtures of fatty acid methyl esters and showed that smoke opacity and emissions of NO_x and UHC increased with the degree of unsaturation. In addition, a higher degree of unsaturation was found to increase the ignition delay and retard the start of combustion, which is also expected to influence the PM and NO_x emissions. Salamanca et al.[8] examined the effects of chemical composition and the degree of unsaturation of methyl esters on engine emissions and observed that linseed biodiesel produced more PM and UHC than palm biodiesel as a consequence of more unsaturated compounds in its composition, which favor the formation of soot precursors in the combustion zone.

There have also been fundamental studies on the effect of unsaturated bonds on NO_x and polycyclic aromatic hydrocarbon (PAH) formation. Garner et al.[9,10] performed shock tube experiments on the pyrolysis and oxidation of *n*-heptane (n-C_7H_{16}), 1-heptene (1-C_7H_{14}), methyl octanoate (C9:0), and

Received: October 12, 2012
Revised: December 11, 2012
Published: December 18, 2012

methyl *trans*-2-octenoate (C9:1) fuels and observed that higher NO can be related to the presence of double bonds in the molecular structure of unsaturated fuels, namely, 1-heptene and methyl octenoate. Note that *n*-heptane and 1-heptene represent, respectively, the hydrocarbon side chain of the surrogate biodiesel esters, methyl octanoate and methyl octenoate. Using detailed kinetic models, Garner et al.[11] further demonstrated the coupling between the increased acetylene (C_2H_2), formed from unsaturated fuels, and the higher prompt NO formed under fuel-rich conditions. Acetylene is also a good precursor for PAH and soot formation. Sarathy at el.[12] compared two fatty acid methyl esters, methyl butanoate and its unsaturated counterpart methyl crotonate, in opposed flow diffusion flame and jet stirred reactor. Methyl crotonate was observed to produce higher C_2H_2, 1-C_3H_4, 1-C_4H_8, 1,3- C_4H_6, and benzene, indicating the potential of increased soot formation with unsaturated biodiesel fuels compared to the saturated ones, although soot emission is reduced with biodiesel compared to petrodiesel due to the presence of oxygen in biodiesel and the significantly higher amount of aromatics in petrodiesel.

To summarize, previous engine studies using various biodiesel fuels report a correlation between the increased NO_x emissions and the degree of unsaturation in the fuel molecular structure. However, they provide conflicting results concerning the effect of unsaturated bonds on soot emissions. This may be due to the strong coupling of various physical and chemical effects caused by the presence of unsaturated bonds. For instance, the fuel chemical structure is known to influence the fuel injection, atomization, vaporization, and ignition delay processes in diesel engines and, consequently, their combustion and emission characteristics. This emphasizes the need for more fundamental studies to isolate the effects of unsaturated bonds on NO_x and soot emissions. Although there have been investigations examining the chemical consequences of unsaturated bonds, their observations have been specific to highly diluted, homogeneous fuel−air mixtures, typical of shock tube and jet stirred reactor environments. Relatively little work has been reported dealing with these aspects in well-characterized flame environments. Fu et al.[13] reported a numerical investigation on NO_x emissions in *n*-heptane and 1-heptene partially premixed double flames. Results indicated that the β-scission and oxidation reactions related to the double C═C bond led to increased NO formation in 1-heptene flames relative to that in *n*-heptane flames. Moreover, differences in NO formation between the two fuels were found to be more pronounced as the level of partial premixing was increased. Analysis of the NO production pathways indicated that the NO is formed mainly through the prompt NO and N_2O intermediate mechanisms, rather than through the thermal and NNH mechanisms.

The present work extends the above study to examine the effect of the presence of a double bond on both NO_x and PAH formation in triple flames burning prevaporized *n*-heptane and 1-heptene fuels. The study is motivated by several considerations. The first is that fundamental flame investigations dealing with large hydrocarbons have mostly considered saturated fuels, such as heptane.[14−18] Another motivation is due to the importance of triple flames in numerous practical applications. Such flames play a fundamental role in characterizing lifted jet flames[19−21] as well as the propagation and stabilization of laminar and turbulent flames.[22,23] Such flames are also relevant to diesel engine combustion, especially in the context of novel low-temperature combustion concepts, including homogeneous charge compression ignition (HCCI),[24] premixed charge compression ignition (PCCI),[25] and dual-fuel injection. Whereas triple flames burning smaller hydrocarbon fuels have been extensively investigated, there have been few studies dealing with large hydrocarbon fuels. Guo and Smallwood[16] numerically investigated *n*-heptane triple flames and observed that a large amount of prompt NO is formed in the rich premixed flame branch. They also discussed interactions involving heat and species transport between the three reaction zones. Briones et al.[26] investigated these interactions and their effects on NO_x emissions in methane−air double and triple flames and concluded that triple flames may have an advantage in reducing NO_x emission over the corresponding premixed flames and double flames.

In this paper, we report a numerical investigation on the structure and emission characteristics of *n*-heptane and 1-heptene triple flames. A triple flame is characterized by the existence of lean premixed, rich premixed, and nonpremixed reaction zones, which are spatially separated but strongly coupled through the transport and chemical kinetic. Therefore, our major objective is to elucidate the effect of the presence of the double bond on NO_x and PAH emissions in partially premixed flames containing regions of lean premixed, rich premixed, and nonpremixed combustion. Moreover, using a counterflow geometry, the spatial separation between the three reaction zones can be controlled by varying the strain rate and the lean and rich equivalence ratios. Consequently, this configuration facilitated a detailed analysis of NO_x and PAH formation processes in each of the three reaction zones. In addition, the differences between the pathways associated with the fuel-rich oxidation of *n*-heptane and 1-heptene and leading to the formation of NO_x and benzene can be analyzed.

2. PHYSICAL−NUMERICAL MODEL

n-Heptane and 1-heptane triple flames in a counterflow configuration were simulated using the Chemkin and OPPDIF packages.[27,28] The configuration involves two opposing jets, one issuing a fuel-lean mixture and the other a fuel-rich mixture. The triple-flame structure and the spatial separation between the three reaction zones are controlled by varying the global strain rate and the fuel-lean (Φ_L) and fuel-rich (Φ_R) equivalence ratios. The global strain rate is defined as

$$a_g = \frac{2v_R}{L}\left(1 + \frac{v_L\sqrt{\rho_L}}{v_R\sqrt{\rho_R}}\right) \quad (1)$$

Here v_R and v_L denote, respectively, the inlet flow velocities of the rich and lean streams, and L is the distance between the two nozzles. Because the gravitational effect is not considered, rich and lean mixtures can be introduced from either nozzle. In the present study, the fuel-lean mixture is issuing from the left nozzle and the fuel-rich mixture from the right nozzle. In addition, L is taken as 2 cm, the pressure as 1 atm, and the temperature of both streams as 400 K. The temperature value is based on the consideration that a mixture of prevaporized fuel and air was used in both streams and that the previous experimental study[15] dealing with *n*-heptane partially premixed flames considered this temperature for the fuel stream.

The kinetic mechanism used to model the *n*-heptane and 1-heptene oxidation chemistry is due to Ranzi et al.[29,30] The mechanism has been previously validated by Shimizu et al.[31] and Frassoldati et al.[32] The NO_x formation is modeled using

the detailed thermal, prompt, N_2O intermediate, and NNH intermediate mechanisms.[33,34] Details are provided in an earlier study.[13] The mechanism also includes the formation and oxidation of benzene and PAHs up to $C_{25}H_{20}$. The combined mechanism consists of 198 species and 4932 reactions. As discussed in the cited studies, the thermal NO route is important at high temperatures (above 1800 K), whereas prompt NO is relevant in rich flames over a wide temperature range. The N_2O and NNH routes have been found to be important under low-temperature conditions.[35−39] Löffler et al.[37] studied natural gas combustions and found that the N_2O route is important under lean conditions at temperatures below 1600 K, whereas the NNH route is important under rich conditions due to high H radical concentration. Konnov et al.[40] simulated hydrogen combustion in well-stirred reactors and observed that the NNH route is also important under lean and stoichiometric conditions at 1500 K.

To quantify the relative contributions of various NO mechanisms, we isolated each mechanism by removing the initiating reactions associated with the other three mechanisms. The initiating reactions are the ones in which nitrogen reacts directly to form the relevant species. Thus, the initiating reaction for thermal NO is

$$N_2 + O \Leftrightarrow N + NO$$

The main initiating reactions for prompt NO are

$$CH + N_2 \Leftrightarrow HCN + N$$

$$CH_2 + N_2 \Leftrightarrow HCN + NH$$

$$C + N_2 \Leftrightarrow CN + N$$

The main initiating reactions for the N_2O intermediate mechanism are

$$N_2 + O(+M) \Leftrightarrow N_2O(+M)$$

$$N_2O + H \Leftrightarrow N_2 + OH$$

$$N_2O + O \Leftrightarrow N_2 + O_2$$

$$N_2O + OH \Leftrightarrow N_2 + HO_2$$

The main initiating reactions for the NNH intermediate mechanism are

$$NNH \Leftrightarrow N_2 + H$$

$$NNH + M \Leftrightarrow N_2 + H + M$$

$$NNH + O_2 \Leftrightarrow HO_2 + N_2$$

$$NNH + O \Leftrightarrow OH + N_2$$

$$NNH + H \Leftrightarrow H_2 + N_2$$

$$NNH + OH \Leftrightarrow H_2O + N_2$$

There are some additional reactions associated with these mechanisms that also involve the conversion of N_2. These are removed together with the main initiating reactions.

Various triple flames were simulated by varying Φ_R, Φ_L, v_R, and v_L for each fuel at a global strain rate of 150 s^{-1} and a global equivalence ratio of $\Phi = 1.1$. To specify conditions for a given flame, we first select Φ_R and Φ_L values and then determine v_R and v_L using eq 1 and the following equation for the global Φ

$$v_R\chi_{F,R} + v_L\chi_{F,L} = (v_R\chi_{O,R} + v_L\chi_{O,L})\Phi\nu \quad (2)$$

Here ν is the stoichiometric fuel/oxygen ratio, $\chi_{F,R}$ and $\chi_{F,L}$ are the fuel mole fractions in rich and lean mixtures, respectively, and $\chi_{O,R}$ and $\chi_{O,L}$ are the oxygen mole fractions in rich and lean mixtures, respectively. Table 1 lists the conditions for the four *n*-heptane and 1-heptene triple flames simulated in this study. The global strain rate for these four flames was specified as 150 s^{-1}. The effect of strain rate on NO_x and PAH formation was also examined by simulating Flames A1 and B1 at strain rates of 150, 250, and 500 s^{-1}.

Table 1. Conditions with Respect to Equivalence Ratio and Velocity of the Rich and Lean Fuel Streams for the Various Triple Flames Simulated

flame	fuel	Φ_R	Φ_L	v_R(cm/s)	v_L(cm/s)	a_g (s^{-1})
A1	*n*-heptane	1.5	0.8	85.7	63.3	150
B1	1-heptene	1.5	0.8	85.7	63.3	150
A2	*n*-heptane	2.0	0.5	88.3	59.7	150
B2	1-heptene	2.0	0.5	88.3	59.8	150
A3	*n*-heptane	2.5	0.4	97.6	50.2	150
B3	1-heptene	2.5	0.4	97.5	50.2	150
A4	*n*-heptane	3.0	0.35	104.6	43.0	150
B4	1-heptene	3.0	0.35	104.5	43.0	150
A1*	*n*-heptane	1.5	0.8	142.9	105.5	250
B1*	1-heptene	1.5	0.8	142.8	105.5	250
A1**	*n*-heptane	1.5	0.8	285.7	211.1	500
B1**	1-heptene	1.5	0.8	285.8	211.0	500

3. RESULTS AND DISCUSSION

Figure 1 presents the temperature and NO profiles for the two *n*-heptane and 1-heptene triple flames simulated at conditions corresponding to A1, B1, A2, and B2 flames in Table 1. The *n*-heptane and 1-heptene flames exhibit similar global structures. For both fuels, the flame is characterized by the existence of a lean premixed (LP) reaction zone located on the left of the stagnation plane, a rich premixed (RP) reaction on the right of the stagnation plane, and a nonpremixed (NP) reaction zone near the stagnation plane. The peak temperature occurs in the NP zone and is slightly higher (ΔT_{max} < 50 K) in 1-heptene flames compared to that in *n*-heptane flames. This can be attributed to the higher enthalpy of formation[41] and therefore higher adiabatic flame temperature for 1-heptene. In addition, comparison of the profiles in panels a and b of Figure 1 indicates that as the level of partial premixing is reduced by simultaneously increasing Φ_R and lowering Φ_L (i.e., flames A2 and B2), both the LP and RP zones move closer to the stagnation plane. This is due to the reduction in flame speeds associated with the LP and RP reaction zones. Comparison of the NO profiles indicates notable differences in NO_x emissions from the *n*-heptane and 1-heptene flames. The amount of NO formed in each of the three reaction zones is higher in 1-heptene flames compared to that in *n*-heptane flames. Moreover, as discussed next, the relative contributions of various NO formation routes are different in the three reaction zones.

3.1. Contributions of Various NO Formation Routes.

Figure 2 compares the relative NO contributions from the prompt, thermal, N_2O, and NNH mechanisms for the two *n*-heptane and 1-heptene flames discussed above. For these flames, the thermal mechanism appears to be the dominant source of NO, although contributions from the other three mechanisms are also significant. Moreover, the relative

dx.doi.org/10.1021/ef301671q | Energy Fuels 2013, 27, 537−548

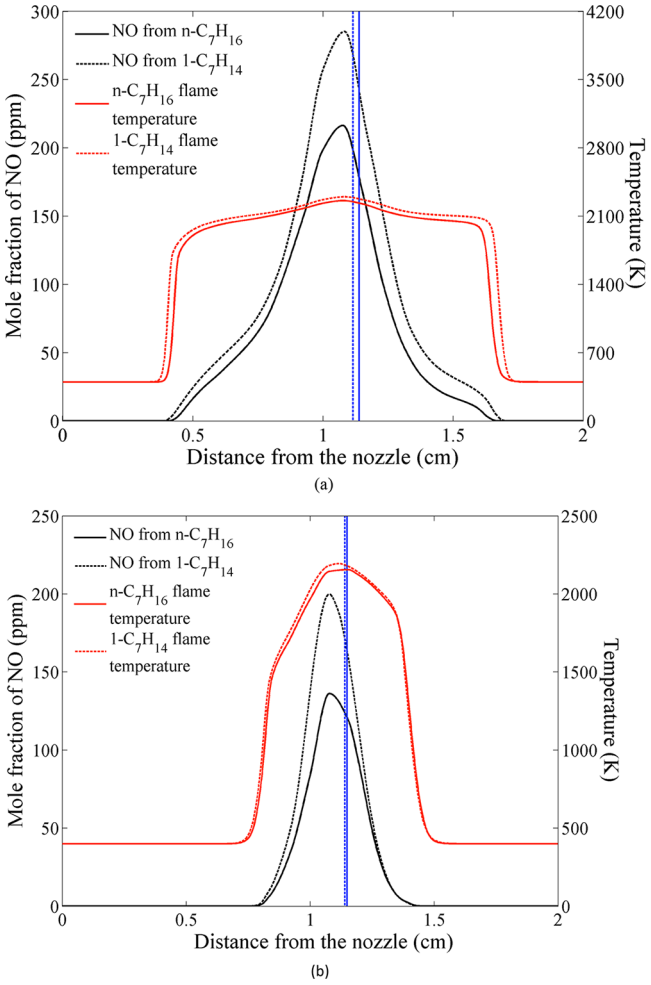

Figure 1. Comparison of temperature and NO profiles in *n*-heptane and 1-heptene flames: (a) flames established at $\Phi_R = 1.5$ and $\Phi_L = 0.8$; (b) flames established at $\Phi_R = 2.0$ and $\Phi_L = 0.5$. Solid lines represent *n*-heptane flames (flames A1 and A2), whereas dashed lines represent 1-heptene flames (flames B1 and B2). Vertical lines indicate the stagnation plane.

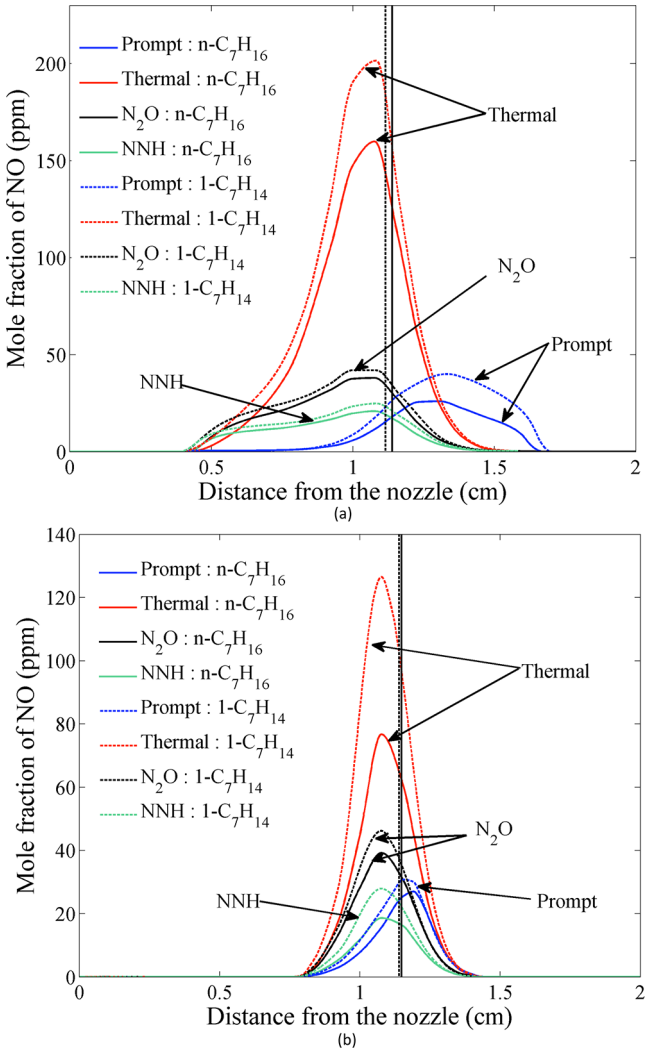

Figure 2. NO profiles corresponding to the thermal, prompt, N_2O intermediate, and NNH mechanisms for *n*-heptane and 1-heptene flames: (a) flames A1 and B1; (b) flames A2 and B2. Solid and dashed lines represent *n*-heptane and 1-heptene flames, respectively. Vertical lines indicate the stagnation plane.

contributions of various mechanisms are different in each reaction zone. NO formation in the RP zone is primarily due to the prompt route, whereas that in the NP zone is dominated by the thermal route. In contrast, NO in the LP zone is formed mainly through the NNH and N_2O routes, with some additional contribution from the thermal route. This is shown more clearly in Figure 3, which plots the rate of production of total NO and those of prompt, thermal, N_2O intermediate, and NNH intermediate mechanisms in flames A1 and B1. As indicated in this figure, thermal NO has the highest production rate in the NP reaction zone where the temperature is the highest. However, the thermal NO production rate is also significant in the LP zone as well as in the region between the LP and NP reaction zones. This is due to the abundance of O radical in the LP zone and the transport of heat from the NP zone to the LP zone. In contrast, the thermal NO production rate is negligible in the RP zone, although the temperature in this zone is relatively high. This is because of the low concentrations of O and OH in this zone, as these species react with N_2 and N through reactions $O + N_2 \rightarrow NO + N$, $N + O_2 \rightarrow NO + O$, and $N + OH \rightarrow NO + O$ to form thermal NO. Note that the peak rate of production of total NO is lower than the sum of the peak rates of four mechanisms simply because the peak of each mechanism is located at a different position in the flame.

Figure 3 further indicates that most of the prompt NO is produced in the RP zone, due to the abundant hydrocarbon radicals in this region. As shown in Figure 4, C_2H_2 and CH concentrations are highest in this region, where the prompt NO is formed through the reaction of CH with N_2. Also note that both the peak prompt NO production rate and the peak CH concentration are located near $x = 1.6$ cm from the fuel-lean nozzle. In addition, as indicated in Figure 3, NO formation in the lean premixed reaction zone occurs mainly through the NNH and N_2O routes. In fact, the NNH concentration is higher in the RP zone than in the LP zone, as shown in Figure 5. However, O radicals are more abundant in the LP zone and can support the key reaction $NNH + O \rightarrow NH + NO$. In contrast, the N_2O concentration is significantly higher in the LP zone, where N_2O is formed through $N_2 + O + M \rightarrow N_2O + M$. Moreover, because these reactions are not directly related to hydrocarbon species (C_2H_2 and CH), the slightly higher NO formed through the NNH and N_2O routes in the LP zone of 1-

dx.doi.org/10.1021/ef301671q | *Energy Fuels* 2013, 27, 537−548

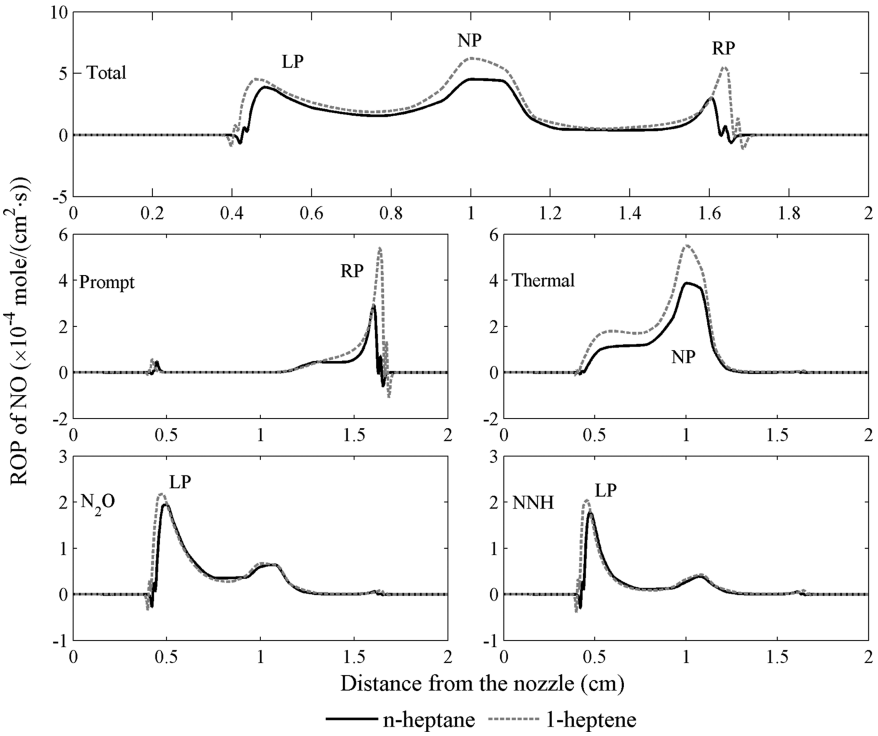

Figure 3. Rate of production of total NO as well as of prompt, thermal, N_2O intermediate, and NNH intermediate NO in flames A1 and B1.

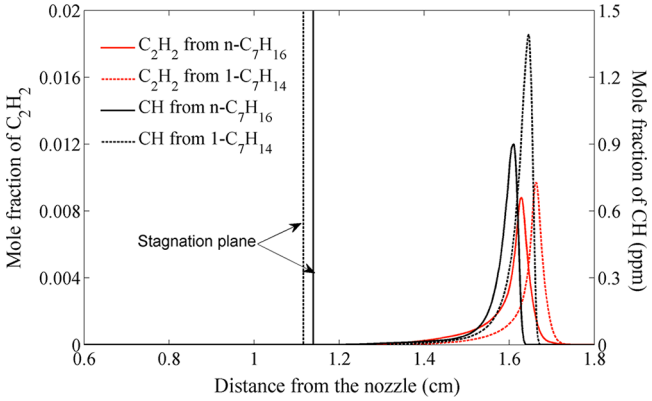

Figure 4. C_2H_2 and CH profiles in flames A1 and B1. Vertical lines represent the stagnation plane.

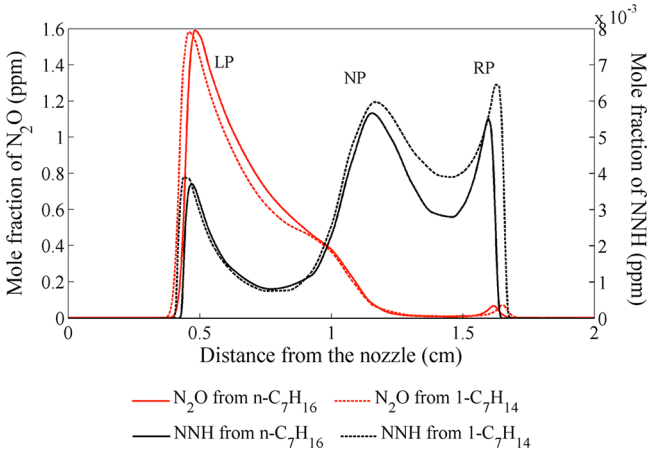

Figure 5. N_2O and NNH profiles in flames A1 and B1.

heptene flame compared to *n*-heptane flame may be due to the higher temperature of the 1-heptene flame.

Another important observation from Figure 3 is the higher prompt NO in the 1-heptene flame (B1) compared to that in the *n*-heptane flame (A1). This is largely due to the higher concentrations of C_2H_2 and CH in the rich premixed region of the 1-heptene flame, as indicated in Figure 4. Moreover, the higher total NO formed in the 1-heptene flame than in the *n*-heptane flame is mainly due to the thermal and prompt contributions; the NNH and N_2O contributions are nearly the same in the two flames. The higher thermal NO formed in the 1-heptene flame is due to the higher temperature in this flame, whereas the higher prompt NO in 1-heptene flame is due to the higher CH concentration. Further discussion on the effect of fuel molecular structure on NO_x formation is provided in a later section.

The relative contributions of the various NO formation routes in each reaction zone of a triple flame depend strongly on the level of premixing or stoichiometries of the fuel-lean and fuel-rich mixtures. This can be seen clearly from the comparison of NO contributions from the prompt, thermal, N_2O, and NNH mechanisms in flames A2 and B2 (Φ_R = 2.0 and Φ_L = 0.5), shown in Figure 6, and in flames A1 and B1 (Φ_R = 1.5 and Φ_L = 0.8), shown in Figure 3. In flames A2 and B2, the LP and RP zones, which are located 0.8 and 1.4 cm from the fuel-lean nozzle (cf. Figure 1b), are relatively weak compared to the NP reaction zone. Consequently, as indicated in Figure 6, most of the NO through the thermal, N_2O, and NNH routes is formed near this reaction zone, while the prompt NO is formed in the region between the RP and NP reaction zones. These aspects are further discussed in the next section.

3.2. Effect of Double Bond on NO Formation. Some insight regarding the effect of the double bond on prompt NO formation can be gained from the C_2H_2 and CH profiles

dx.doi.org/10.1021/ef301671q | *Energy Fuels* 2013, 27, 537−548

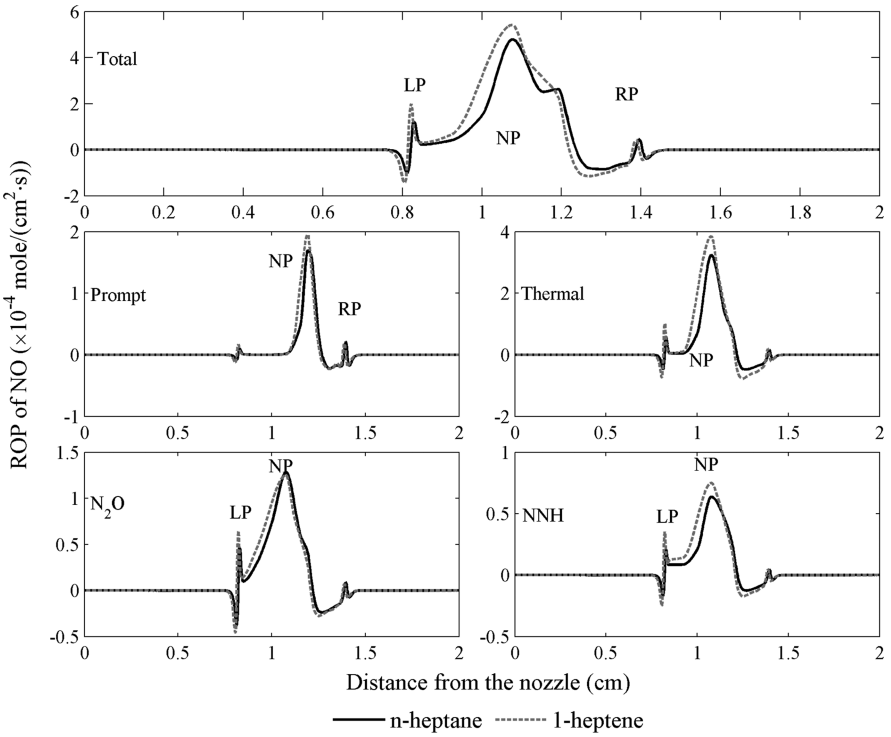

Figure 6. Rate of production of total NO and of prompt, thermal, N_2O intermediate, and NNH intermediate NO in flames A2 and B2.

presented in Figure 7 for flames A2 and B2. Whereas the C_2H_2 profile contains one peak in the RP zone, the CH profile shows

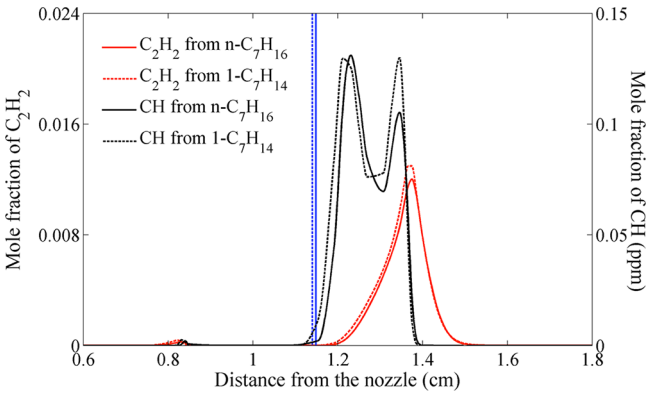

Figure 7. C_2H_2 and CH profiles in flames A2 and B2. Vertical lines represent the stagnation plane.

two peaks, one in the RP zone and the other in the region between the RP and NP zones. The second peak is due to the incomplete conversion of C_2H_2 to CH in the rich premixed zone. Note that the CH peak in the rich premixed zone is significantly higher in the 1-heptene flame than in the *n*-heptane flame, whereas the second peak shows very little difference between the two fuels. Between these two peaks, the reactions producing CH slow due to the very low concentrations of O and H radicals there. The chemistries that dominate the regions of the two peaks of CH are different. In the RP zone, the decomposition of the original fuel molecule into smaller species plays an important role. 1-Heptene produces more C_2H_2 and thus more CH in the first peak compared to *n*-heptane. This is consistent with the fact that the first peak of CH is formed right after the peak of C_2H_2. However, the conversion of C_2H_2 to CH is only partially completed. Consequently, a second peak is formed downstream of the first peak. However, the effect of the double-bond chemistry of 1-heptene is diminished in this region, because the large hydrocarbon molecules are already broken down in the rich premixed zone. Because most of the prompt NO is produced in the region between the two reaction zones and not in the rich premixed zone, the effect of the double-bond fuel on prompt NO formation is reduced for this flame.

3.3. Effect of Partial Premixing and Strain Rate on NO_x Emission Index. Figure 8 plots the emission index of total NO

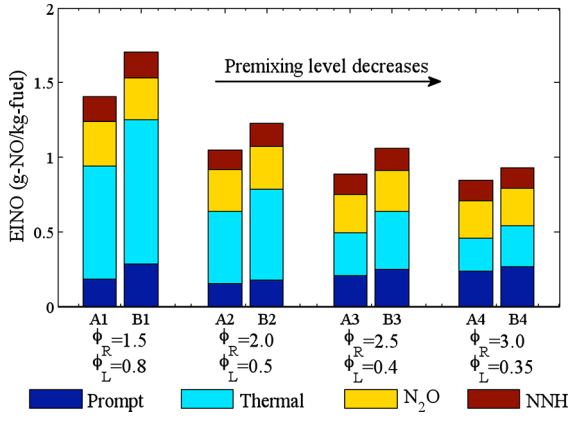

Figure 8. Emission index for the total NO and for the prompt, thermal, N_2O, and NNH mechanisms for the four *n*-heptane and 1-heptene triple flames, all at a global strain rate of a_g = 150 s^{-1} and a global equivalence ratio of Φ = 1.1. Each two neighboring bars represent *n*-heptane (left) and 1-heptene (right) flames, respectively, at the same conditions. The level of premixing for the four flames decreases going from left to right along the "flame number" axis. Φ_L and Φ_R values for these flames are given in Table 1.

dx.doi.org/10.1021/ef301671q | *Energy Fuels* 2013, 27, 537−548

(EINO) and of the prompt, thermal, N_2O, and NNH mechanisms for the four *n*-heptane and 1-heptene triple flames. All of these flames are simulated at a global strain rate of a_g = 150 s^{-1} and a global equivalence ratio of Φ = 1.1. Results concerning the effect of stain rate on the triple-flame structure

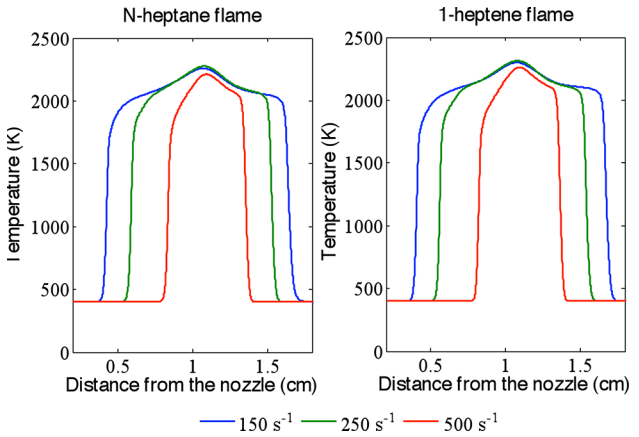

Figure 9. Temperature profiles for *n*-heptane and 1-heptene triple flames at different strain rates, ϕ_L = 0.8 and ϕ_R = 1.5.

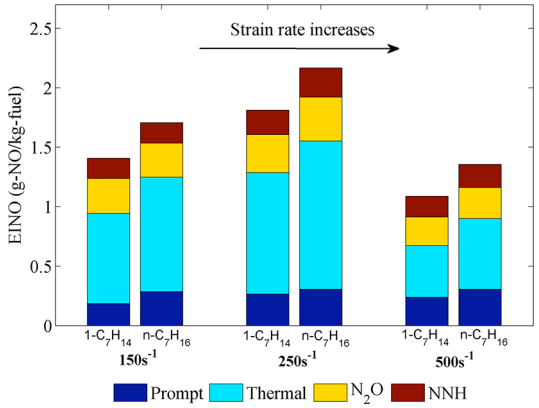

Figure 10. Emission index for the total NO and for the prompt, thermal, N_2O, and NNH mechanisms for the four *n*-heptane and 1-heptene triple flames at global strain rates of a_g = 150 , 250, and 500 s^{-1}, ϕ_L = 0.8, and ϕ_R = 1.5.

and NO_x emission are shown in Figures 9 and 10. The emission index of NO is defined as

$$\mathrm{EINO} = \frac{\int_0^L \mathrm{MW_{NO}}\dot{\omega}_{\mathrm{NO}}\,\mathrm{d}x}{-\int_0^L \mathrm{MW_{fuel}}\dot{\omega}_{\mathrm{fuel}}\,\mathrm{d}x}$$

There are several observations from Figure 8. First, 1-heptene flames have higher EINO than *n*-heptane flames for all four cases. The EINO values for the thermal, prompt, and NNH mechanisms are also higher for 1-heptene compared to *n*-heptane, whereas those for the N_2O mechanism are essentially the same for the two fuels. Second, as the level of premixing is reduced (going from left to right), the total EINO decreases for both fuels. The difference in EINO between the two fuels also decreases as the level of premixing is reduced. However, the relative contributions of various NO routes to total EINO exhibit a more complex behavior. As the level of premixing is reduced, the contribution of thermal EINO decreases significantly, whereas those of prompt and NNH increase and that of N_2O remains about the same. It is also important to note that the variation of prompt EINO with the level of premixing correlates with the peak CH mole fraction.

Figure 9 presents the temperature profiles for *n*-heptane and 1-heptene triple flames established at strain rates of 150, 250, and 500 s^{-1}, ϕ_L = 0.8, and ϕ_R = 1.5. As the strain rate is increased, the peak flame temperature, which occurs in the NP zone, first increases slightly and then decreases. This is due to the competing effects of reduced residence time at higher strain rates and enhanced interaction between the NP zone and the two premixed zones. As discussed by Guo et al.,[42] as the strain rate is increased, the physical separation between the reaction zones is reduced (cf. Figure 9), which leads to enhanced interaction between the NP and two premixed reaction zone and, thus, slightly higher temperature for the strain rate of 250 s^{-1}. This can be explained through the effect of Lewis numbers (Le) in the rich (RP) and lean premixed (LP) reaction zones, which are, respectively, greater and less than unity in the two zones. The Le less than unity in the RP zone implies increased transport of CO and H_2 from the RP zone into the NP zone and, thus, slightly higher temperature in the NP zone for the intermediate strain rate. The effect of strain rate on NO formation is depicted in Figure 10, which plots the emission index of total NO and of prompt, thermal, N_2O, and NNH mechanisms for the *n*-heptane and 1-heptene triple flames at different strain rates. An important observation is the higher NO emission in 1-heptene flames compared to that in *n*-heptane flames irrespective of the strain rate. Moreover, as the strain rate is increased, the EINO first increases and then decreases, consistent with the variation of peak flame temperature with strain rate. The EINO values for the prompt, thermal, N_2O, and NNH mechanisms also follow a similar trend. However, the relative contribution of prompt NO becomes more pronounced at higher strain rates, whereas that of thermal NO is reduced to the reduced residence time.

3.4. Effect of Double Bond on PAH Formation. The effect of the unsaturated bond on soot emission is examined in terms of the benzene profiles in *n*-heptane and 1-heptene triple flames. The capability of the simulation model for predicting benzene and larger PAH species, including naphthalene ($C_{10}H_8$), phenanthrene ($C_{14}H_{10}$), and pyrene ($C_{16}H_{10}$), has been demonstrated in our previous study.[14] Moreover, the cited study has shown a direct correlation between the amounts of benzene and larger PAH species. Figures 11 and 12 present benzene profiles for the various *n*-heptane and 1-heptene triple flames established at different levels of premixing and strain rates. An important observation from these figures is the significantly higher benzene formation in 1-heptene flames compared to that in *n*-heptane flames. As discussed in the following, this can be attributed to the effect of the double bond on the 1-heptene oxidation chemistry, leading to the increased formation of allyl radical (C_3H_5), 1,3-butadiene (C_4H_6), propargyl (C_3H_3), and other precursors, and thus significantly higher benzene formation in 1-heptene flames. It is also important to note that most of the benzene is formed in the RP zone, which is characterized by high concentrations of intermediate hydrocarbons, such as C_3H_5, C_4H_6, and C_3H_3. With regard to the effect of strain rate, results indicate that the amount of PAH formed in 1-heptene flames is consistently higher than that in *n*-heptane flames irrespective of the strain rate.

dx.doi.org/10.1021/ef301671q | *Energy Fuels* 2013, 27, 537−548

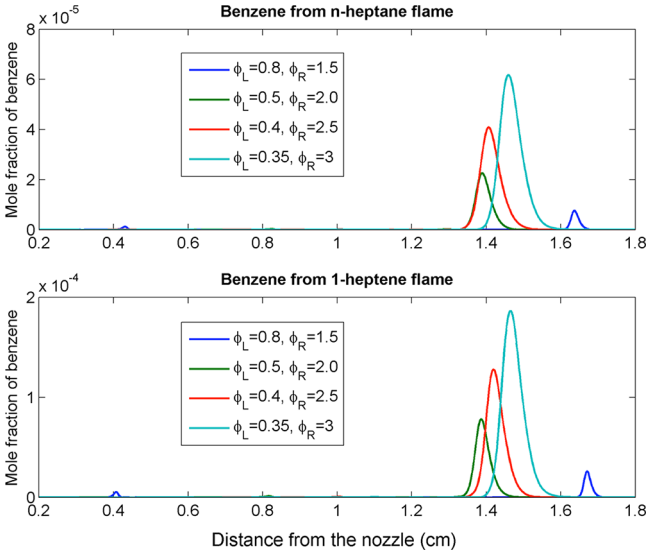

Figure 11. Benzene profiles in *n*-heptane and 1-heptene flames established at different levels of partial premixing. Strain rate is 150 s^{-1}.

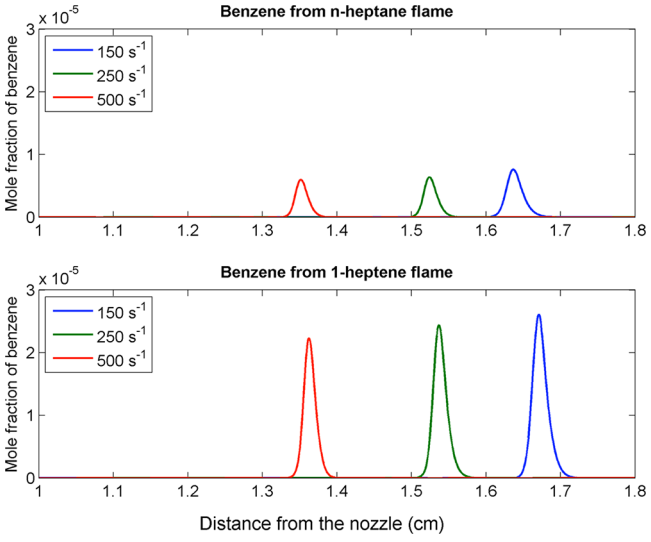

Figure 12. Benzene profiles in *n*-heptane and 1-heptene flames established at different strain rates, ϕ_L = 0.8, and ϕ_R = 1.5.

Figure 13 presents the emission indices of benzene and naphthalene for the four *n*-heptane and 1-heptene triple flames discussed in the context of Figure 10. As the level of premixing is reduced, the PAH emission indices increase for both fuels. This is due to the increasingly higher amounts of intermediate hydrocarbons (C_3H_5, C_3H_3, and C_4H_6) formed and the lack of oxidizer in the RP zone. In addition, for all four cases of premixing, the PAH emission from 1-heptene flames is significantly higher than that from *n*-heptane flames.

To gain further insight into the effect of the double bond on PAH formation, a reaction pathway analysis was performed, and the results are summarized in Figure 14, which presents the dominant pathways for the formation of benzene in 1-heptene and *n*-heptane flames, respectively, at ϕ_L = 0.8, ϕ_R = 1.5, and a strain rate of 150 s^{-1}. Whereas the oxidation of these two fuels follows different paths depending upon the temperature, benzene is mainly formed through the recombination reaction of propargyl radicals (C_3H_3).[43] Most of the C_3H_3 is formed from allyl radicals (C_3H_5), and the formation of allyl from fuel

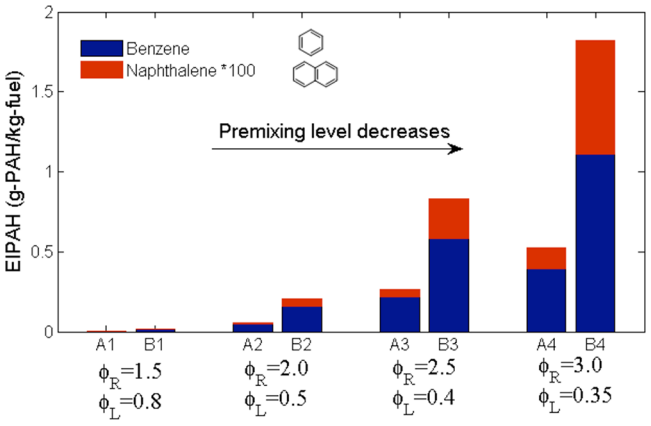

Figure 13. Emission index of benzene and naphthalene for the four *n*-heptane and 1-heptene triple flames, all at a global strain rate of a_g = 150 s^{-1} and a global equivalence ratio of Φ = 1.1. Each two neighboring bars represent *n*-heptane (left) and 1-heptene (right) flames, respectively, at the same conditions. The level of premixing for the four flames decreases from left to right along the "flame number" axis. Φ_L and Φ_R values for these flames are given in Table 1.

decomposition is quite different for 1-heptene and *n*-heptane fuels, as can be seen on the left side of Figure 14. At high temperatures (>1200 K), typical of flame environment, most of the 1-heptene directly decomposes into C_3H_5 and C_4H_9. In contrast, the decomposition of *n*-heptane at high temperature mostly involves C−C fission, forming various alkyl radicals, such as CH_3, C_6H_{13}, C_2H_5, C_5H_{11}, C_3H_7, and C_4H_9, most of which then decompose into C_2H_4 and CH_3 (not shown) through β scission and H abstraction reactions. Similarly, the butyl (C_4H_9) formed from 1-heptene also decomposes into C_2H_4. In fact, this is the main source of ethylene in the 1-heptene flame (cf. Figure 14a), whereas there are multiple alkyl species (C_6H_{13}, C_5H_{11}, C_4H_9, C_3H_7, etc.) that form ethylene in the *n*-heptane flame (cf. Figure 14b). Consequently, the ethylene concentration is higher in the *n*-heptane flame compared to that in the 1-heptene flame, as indicated in Figure 15. Ethylene subsequently forms vinyl (C_2H_3), which can also produce benzene through its reaction with butadiene. However, the higher C_2H_4 concentration does not imply increased benzene production in the *n*-heptane flame, because the butadiene concentration is much lower in this flame compared to that in the 1-heptene flame, as shown in Figure 15. This aspect is further discussed in the following.

As indicated in Figure 14, the low-temperature (<1200 K) oxidation paths of *n*-alkane and 1-alkene are also significantly different. The decomposition of *n*-heptane is initiated by H abstraction forming *n*-alkyl radicals, which then break into various 1-alkenes (C_3H_6, C_4H_8, C_5H_{10}) and smaller alkyls (CH_3 to C_5H_{11}) through β scission and H abstraction reactions. The smaller alkyls subsequently form C_2H_4, which leads to the production of benzene through vinyl (C_2H_3), similar to the high-temperature reaction path discussed above. The various 1-alkanes (except C_2H_4), on the other hand, represent the main source of allyl and butadiene, which subsequently form benzene. However, the formation of allyl competes with that of butadiene in *n*-heptane flames, unlike the case for 1-heptene flames (discussed below), in which the path to butadiene is preferred. Consequently, the amount of butadiene formed in *n*-heptane flames is significantly lower than that in 1-heptene flames (cf. Figure 15), as stated earlier. The low-temperature

dx.doi.org/10.1021/ef301671q | Energy Fuels 2013, 27, 537−548

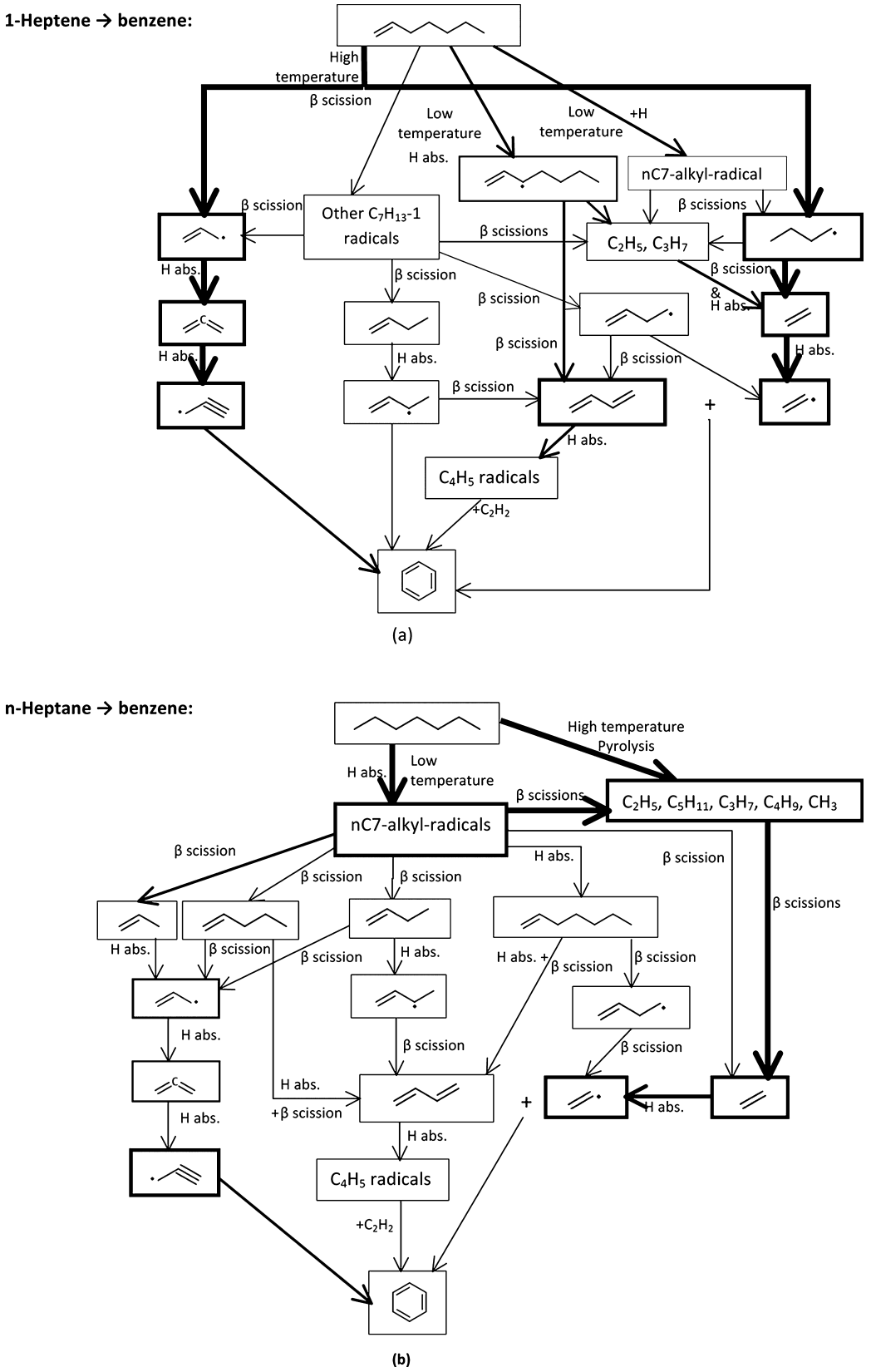

Figure 14. Benzene formation pathways in *n*-heptane and 1-heptene flames.

oxidation of 1-heptene follows three different paths. The main path involves H abstraction at the α-carbon location near the double bond, forming 1-butylallyl radicals, which then break into 1,3-butadiene and propyl. The second path involves H addition and formation of *n*-C7 alkyl radicals, which then follow a path similar to that for *n*-heptane discussed above. The third path involves the decomposition of 1-heptene through H abstraction from other C−H bonds, forming other 1-C_7H_{13}

dx.doi.org/10.1021/ef301671q | *Energy Fuels* 2013, 27, 537−548

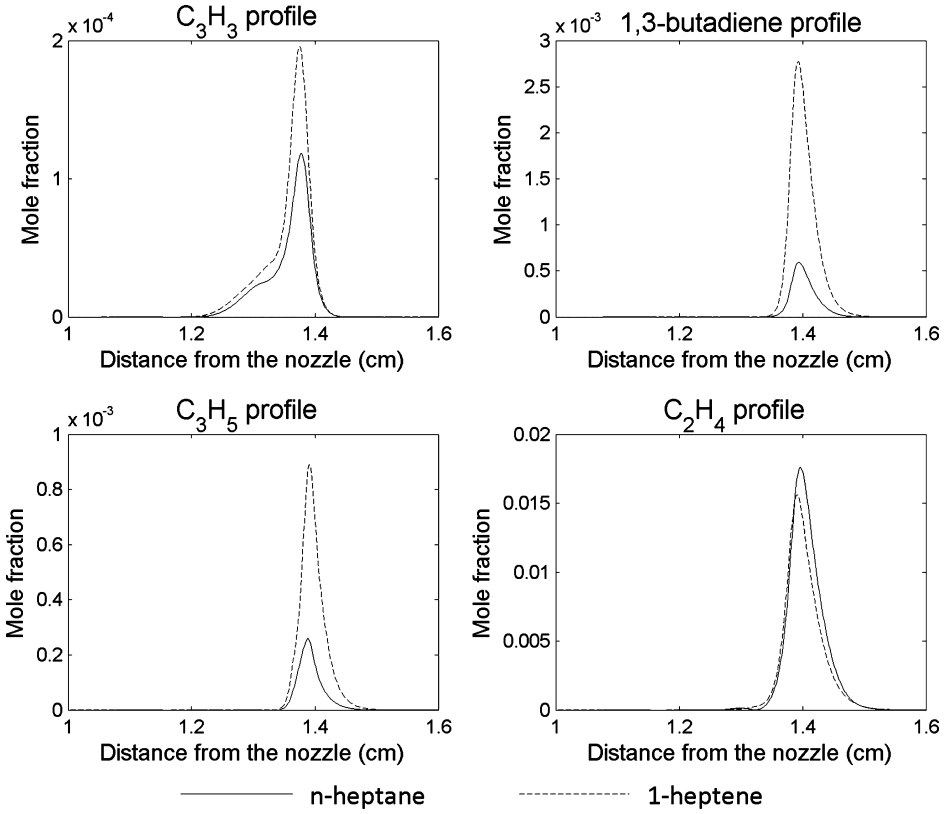

Figure 15. Concentration profiles of benzene precursors C_3H_3, C_3H_5, 1,3-butadiene, and C_2H_4 in *n*-heptane and 1-heptene flames at $\Phi_L = 0.8$, $\Phi_R = 1.5$, and a global strain rate of $a_g = 150\ s^{-1}$.

radicals, which then form propargyl (through allyl) and 1-C_4H_7 and, subsequently, benzene. In summary, for the low-temperature reaction path, *n*-heptane tends to produce more allyl than 1-heptene. However, in the rich premixed flame environment, the benzene formation is dominated by the high-temperature reaction path, with the implication that a significantly higher amount of benzene is formed in 1-heptene flames compared to that in *n*-heptane flames. The above pathway from fuel to benzene formation and the observations regarding the importance of allylic radicals, propargyl, vinyl, and 1,3-butadiene (C_4H_6) are consistent with previous studies; see, for example, Zhang et al.,[44,45] who examined the chemistry of aromatic precursor formation in *n*-heptane premixed flames. Note, however, that the high-temperature reaction pathway was found to be more important for benzene formation in our study.

Finally, it should be mentioned that C_2H_2 is known to be an important precursor for PAH and soot production. As stated earlier, the presence of the double bond leads to the higher production of C_2H_2 in 1-heptene flames than in *n*-heptane flames. In the context of Figure 14, C_2H_2 is mainly formed from vinyl and produces benzene through its reaction with C_4H_5 radicals, which are formed from butadiene. Acetylene subsequently plays an important role in the formation of larger PAH species through the hydrogen abstraction acetylene addition (HACA) mechanism. It is also important to note that whereas the concentration of C_2H_4 is higher in *n*-heptane flames, that of C_2H_2 is higher in 1-heptene flames. This is due to the fact that C_2H_2 is produced from both C_2H_4 (through vinyl) and C_4H_5 (which breaks down to form C_2H_2 and C_2H_3), and the concentration of C_4H_5 is noticeably higher in 1-heptene flames, leading to the increased production of C_2H_2 in these flames.

4. CONCLUSIONS

We have numerically investigated the flame structure and NO_x and PAH emissions in triple flames burning prevaporized *n*-heptane and 1-heptene fuels, which, respectively, represent the hydrocarbon side chain of the two surrogate biodiesel esters, methyl octanoate (C9:0) and methyl octenoate (C9:1). The objective is to examine the effect of the unsaturated (double) bond in the fuel molecular structure on NO_x and soot emissions in a flame environment containing regions of lean premixed, rich premixed, and nonpremixed combustion. A validated detailed kinetic model with 198 species and 4932 reactions has been used to simulate triple flames with different levels of premixing at a fixed global equivalence ratio and different strain rates. The important observations are as follows.

Whereas the global structures of *n*-heptane and 1-heptene triple flames are similar, there are significant differences with respect to NO_x emission from these flames. For all of the cases simulated, the NO_x emission from 1-heptene flames is higher than that from *n*-heptane flames. The NO production rates in each of the three reaction zones, that is, the rich premixed, lean premixed, and nonpremixed zones, are also higher in 1-heptene flames compared to *n*-heptane flames. Moreover, these differences become more pronounced as the level of premixing is increased.

The NO_x formed through the prompt, thermal, N_2O, and NNH mechanisms is also higher in 1-heptene triple flames compared to that in *n*-heptane triple flames. NO_x formation in the rich premixed zone is primarily due to the prompt NO, whereas that in the nonpremixed zone is mainly through the

dx.doi.org/10.1021/ef301671q | *Energy Fuels* 2013, 27, 537−548

thermal route. In contrast, NO_x in the lean premixed zone is formed mostly through the NNH and N_2O mechanisms.

PAH species such as benzene, naphthalene, and pyrene are mostly formed in the rich premixed zone, and their emissions are significantly higher in 1-heptene flames than in *n*-heptane flames. For benzene formation, a detailed analysis of the reaction pathway indicates that the dominant path for benzene formation depends strongly on the fuel type and temperature. The dominant path for benzene formation involves the recombination of propargyl (C_3H_3) radicals, and the presence of the double bond in 1-heptene provides a significant route for its production through the formation of allyl radicals. At temperatures above 1200 K, typical of the environment in the rich premixed zone, a much higher amount of allyl is formed due to the presence of the double bond, and this leads to a significantly higher amount of benzene and larger PAH species in 1-heptene flames.

As the level of premixing level is reduced, NO_x emissions decrease while PAH emissions increase. In addition, the relative contribution of thermal NO decreases, those of prompt and NNH mechanisms increase, and that of N_2O remains about the same, as the level of premixing is reduced.

As the strain rate is increased, the total NO emissions first increase due to the increased interaction between the nonpremixed and premixed reaction zones but subsequently decrease due to the reduced residence time at higher strain rate. Also, the relative contribution of prompt NO to total NO_x increases compared to that of thermal NO. Whereas the PAH emissions decrease with the increase in strain rate, they are significantly higher in 1-heptene flames than in *n*-heptane flames, irrespective of the strain rate.

Future work will focus on examining the effects of unsaturated bonds on NO_x and PAH emissions in triple flames burning long-chain saturated and unsaturated biodiesel surrogates.

AUTHOR INFORMATION

Corresponding Author

*Postal address: Department of Mechanical and Industrial Engineering, University of Illinois at Chicago, 842 W. Taylor St., Chicago, IL 60607, USA. Fax: 1 (312) 413-0441. Phone: 1 (312) 996-2235. E-mail: ska@uic.edu.

Notes

The authors declare no competing financial interest.

REFERENCES

(1) Song, H.; Tompkins, B. T.; Bittle, J. A.; Jacobs, T. J. Comparisons of NO emissions and soot concentrations from biodiesel-fuelled diesel engine. *Fuel* http://dx.doi.org/10.1016/j.fuel.2012.01.004

(2) Graboski, M.; McCormick, R. Combustion of fat and vegetable oil derived fuels in diesel engines. *Prog. Energy Combust. Sci.* **1998**, *24*, 125−164.

(3) McCormick, R. L.; Graboski, M. S.; Alleman, T. L.; Herring, A. M.; Tyson, K. S. Impact of biodiesel source material and chemical structure on emissions of criteria pollutants from a heavy-duty engine. *Environ. Sci. Technol.* **2001**, *35* (9), 1742−1747.

(4) Lapuerta, M.; Herreros, J. M.; Lyons, L. L.; García-Contreras, R.; Briceño, Y. Effect of the alcohol type used in the production of waste cooking oil biodiesel on diesel performance and emissions. *Fuel* **2008**, *87*, 3161−3169.

(5) Puhan, S.; Saravanan, N.; Nagarajan, G.; Vedaraman, N. Effect of biodiesel unsaturated fatty acid on combustion characteristics of a DI compression ignition engine. *Biomass Bioenergy* **2010**, *34*, 1079−1088.

(6) Schönborn, A.; Ladommatos, N.; Williams, J.; Allan, R.; Rogerson, J. The influence of molecular structure of fatty acid monoalkyl esters on diesel combustion. *Combust. Flame* **2009**, *156*, 1396−1412.

(7) Benjumea, P.; Agudelo, J. R.; Agudelo, A. F. Effect of the degree of unsaturation of biodiesel fuels on engine performance, combustion characteristics, and emissions. *Energy Fuels* **2011**, *25* (1), 77−85.

(8) Salamanca, M.; Mondragón, F.; Agudelo, J. R.; Benjumea, P.; Santamaría, A. Variations in the chemical composition and morphology of soot induced by the unsaturation degree of biodiesel and a biodiesel blend. *Combust. Flame* **2012**, *159*, 1100−1108.

(9) Garner, S.; Brezinsky, K. Biologically derived diesel fuel and NO formation: an experimental and chemical kinetic study. *Combust. Flame* **2011**, *158* (Part 1), 2289−2301.

(10) Garner, S.; Dubois, T.; Togbe, C.; Chaumeix, N.; Dagaut, P.; Brezinsky, K. Biologically derived diesel fuel and NO formation: Part 2. Model development and extended validation. *Combust. Flame* **2011**, *158*, 2302−2313.

(11) Garner, S.; Sivaramakrishnan, R.; Brezinsky, K. The high-pressure pyrolysis of saturated and unsaturated C_7 hydrocarbons. *Proc. Combust. Inst.* **2009**, *32*, 461−467.

(12) Sarathy, S. M.; Gaïl, S.; Syed, S. A.; Thomson, M. J.; Dagaut, P. A comparison of saturated and unsaturated C_4 fatty acid methyl esters in an opposed flow diffusion flame and a jet stirred reactor. *Proc. Combust. Inst.* **2007**, *31*, 1015−1022.

(13) Fu, X.; Garner, S.; Aggarwal, S. K.; Brezinsky, K. A numerical study of NO_x emissions from *n*-heptane and 1-heptene counterflow flames. *Energy Fuels* **2012**, *26*, 879−888.

(14) Berta, P.; Puri, I. K.; Aggarwal, S. K. Structure of partially premixed *n*-heptane-air counterflow flames. *Proc. Combust. Inst.* **2005**, *30*, 447−453.

(15) Berta, P.; Aggarwal, S. K.; Puri, I. K. An experimental and numerical investigation of *n*-heptane/air counterflow partially premixed flames and emission of NO_x and PAH species. *Combust. Flame* **2006**, *145*, 740−764.

(16) Guo, H.; Smallwood, G. J. A numerical investigation on NO_x formation in counterflow *n*-heptane triple flames. *Int. J. Thermal Sci.* **2007**, *46*, 936−943.

(17) Smallbone, A. J.; Liu, W.; Law, C. K.; You, X. Q.; Wang, H. Experimental and modeling study of laminar flame speed and non-premixed counterflow ignition of *n*-heptane. *Proc. Combust. Inst.* **2009**, *32*, 1245−1252.

(18) Xue, H.; Aggarwal, S. K. NO_x emissions in *n*-heptane/air partially premixed flames. *Combust. Flame* **2003**, *132*, 723−741.

(19) Cha, M. S.; Chung, S. H. *Symp. (Int.) Combust.* **1996**, *26*, 121−128.

(20) Ghosal, S.; Vervisch, L. Stability diagram for lift-off and blowout of a round jet laminar diffusion flame. *Combust. Flame* **2001**, *123*, 646−655.

(21) Chomiak, J.; Karlsson, A. Flame liftoff in diesel sprays. *Symp. (Int.) Combust.* **1996**, *26*, 2557−2564.

(22) Mansour, M. S. Stability characteristics of lifted turbulent partially premixed jet flames. *Combust. Flame* **2003**, *133*, 263−274.

(23) Joedicke, A.; Peters, N.; Mansour, M. The stabilization mechanism and structure of turbulent hydrocarbon lifted flames. *Proc. Combust. Inst.* **2005**, *30*, 901−909.

(24) Kong, S. C.; Reitz, R. D. Application of detailed chemistry and CFD for predicting direct injection HCCI engine combustion and emissions. *Proc. Combust. Inst.* **2002**, *29*, 663−669.

(25) Babajimopoulos, A.; Assanis, D. N.; Flowers, D. L.; Aceves, S. M.; Hessel, R. P. A fully coupled computational fluid dynamics and multi-zone model with detailed chemical kinetics for the simulation of premixed charge compression ignition engines. *Int. J. Engine Res.* **2005**, *6*, 497−512.

(26) Briones, A. M.; Som, S.; Aggarwal, S. K. Effects of H_2 enrichment on the propagation characteristics of CH_4-air triple flames. *Combust. Flame* **2007**, *149*, 448−462.

(27) Lutz, A. E.; Kee, R. J.; Grear, J. F.; Rupley, F. M. *Sandia National Laboratory*, Report SAND96-8243.

(28) Kee, R. J.; Rupley, F. M.; Miller, J. A. *Sandia National Laboratory*, Report 89-8009B.
(29) Ranzi, E.; Dente, M.; Goldaniga, A.; Bozzano, G.; Faravelli, T. Lumping procedures in detailed kinetic modeling of gasification, pyrolysis, partial oxidation and combustion of hydrocarbon mixtures. *Prog. Energy Combust. Sci.* **2001**, *27*, 99−139.
(30) Goldaniga, A.; Faravelli, T.; Ranzi, E. The kinetic modeling of soot precursors in a butadiene flame. *Combust. Flame* **2000**, *122*, 350−358.
(31) Shimizu, T.; Williams, F. A.; Frassoldati, A. *Proceedings of the 43rd American Institute of Aeronautics and Astronautics (AIAA) Aerospace Science Meeting and Exhibit*, Reno, NV, Jan 10−13; AIAA: Reston, VA, 2005; AIAA-0144.
(32) Frassoldati, A.; Faravelli, T.; Ranzi, E. Kinetic modeling of the interactions between NO and hydrocarbons at high temperature. *Combust. Flame* **2003**, *135*, 97−112.
(33) Miller, J. A.; Bowman, C. T. Mechanism and modeling of nitrogen chemistry in combustion. *Prog. Energy Combust. Sci.* **1989**, *15*, 287−338.
(34) Bozzelli, J. W.; Dean, A. M. O+NNH: a possible new route for NO_x formation in flames. *Int. J. Chem. Kinetics* **1995**, *27*, 1097−1109.
(35) Rørtveit, G. J.; Hustad, J. E.; Li, S. C.; Williams, F. A. Effects of diluents on NO_x formation in hydrogen counterflow flames. *Combust. Flame* **2002**, *130*, 48−61.
(36) Guo, H.; Smallwood, G. J.; Liu, F.; Ju, Y.; Gülder, Ö. L. The effect of hydrogen addition on flammability limit and NO_x emission in ultra-lean counterflow CH_4/air premixed flames. *Proc. Combust. Inst.* **2005**, *30*, 303−311.
(37) Löffler, G.; Sieber, R.; Harasek, M.; Hofbauer, H.; Hauss, R.; Landauf, J. NO_x formation in natural gas combustion—a new simplified scheme for CFD calculations. *Fuel* **2006**, *85*, 513−523.
(38) Glarborg, P.; Alzueta, M. U.; Dam-Johansen, K.; Miller, J. A. Kinetic modeling of hydrocarbon/nitric oxide interactions in a flow reactor. *Combust. Flame* **1998**, *115*, 1−27.
(39) Galletti, C.; Parente, A.; Derudi, M.; Rota, R.; Tognotti, L. Numerical and experimental analysis of NO emissions from a lab-scale burner fed with hydrogen-enriched fuels and operating in MILD combustion. *Int. J. Hydrogen Energy* **2009**, *34*, 8339−8351.
(40) Konnov, A. A.; Colson, G.; Ruyck, J. D. NO formation rates for hydrogen combustion in stirred reactors. *Fuel* **2001**, *80*, 49−65.
(41) Heywood, J. B. *Internal Combustion Engine Fundamentals*; McGraw-Hill: New York, 1988.
(42) Guo, H.; Liu, F.; Smallwood, G. J. A numerical study of laminar methane/air triple flames in two-dimensional mixing layers. *Int. J. Thermal Sci.* **2006**, *45*, 586−594.
(43) Miller, J. A.; Melius, C. F. Kinetic and thermodynamic issues in the formation of aromatic compounds in flames of aliphatic fuels. *Combust. Flame* **1992**, *91*, 21−39.
(44) Zhang, R. H.; Eddings, E. G.; Sarofim, A. F. A journey from *n*-heptane to liquid transportation fuels. 1. The role of the allylic radical and its related species in aromatic precursor chemistry. *Energy Fuels* **2008**, *22* (2), 945−953.
(45) Zhang, R. H.; Eddings, E. G.; Sarofim, A. F. Olefin chemistry in a premixed *n*-heptane flame. *Energy Fuels* **2007**, *21* (2), 677−685.